

Saliency Integration: An Arbitrator Model

Yingyue Xu, Xiaopeng Hong, Guoying Zhao

Department of Computer Science and Engineering, University of Oulu

Abstract—Saliency integration approaches have aroused general concern on unifying saliency maps from multiple saliency models. In fact, saliency integration is a weighted aggregation of multiple saliency maps, such that measuring the weights of saliency models is essential. In this paper, we propose an unsupervised model for saliency integration, namely the arbitrator model (AM), based on the Bayes' probability theory. The proposed AM incorporates saliency models of varying expertise and a prior map based on the consistency of the evidence from multiple saliency models and a reference saliency map from generally accepted knowledge. Also, we suggest two methods to learn the expertise of the saliency models without ground truth. The experimental results are from various combinations of twenty-two state-of-the-art saliency models on five datasets. The evaluation results show that the AM model improves the performance substantially compared to the existing state-of-the-art approaches, regardless of the chosen candidate saliency models.

Index Terms—saliency integration, saliency aggregation.

I. INTRODUCTION

Over the past two decades, saliency detection has hit much attention for its broad applications, such as image and video segmentation [1], video compression [2], and advertising [3]. Aiming at highlighting the regions of interest (ROI) of the human visual system on a scene with biologically plausible cues, a variety of saliency models have been proposed [4]–[24].

Existing saliency models utilize a broad range of strategies such as coarse-to-fine saliency map estimation [23], [25], top-down [10], [26] or bottom-up [4]–[8], [19], [27], [28] feature extraction, making different assumptions, for example, the background surrounding assumption [16], [18], [19], [29], [30], and relying on a variety of models including support vector machine [10], AdaBoost [22], multiple kernel learning [11], [31], and deep convolutional neural networks [20], [21], [24], *etc.*

Recently, integration based approaches arouse broad concern on unifying saliency maps from multiple saliency models, namely saliency integration (or saliency aggregation). Since each saliency model has its advantages and limitations, integration based approaches are proposed to make up the defects of one saliency model via exploiting advantages from the rest models.

The previous works point out that saliency integration is essentially a weighted combination of multiple saliency maps, such that the key point is to acquire the weights of saliency models [32]. Existing saliency integration approaches weigh each saliency map to be combined in two ways: supervised and unsupervised. Supervised saliency integration models [33], [34] learn the weights of candidate saliency models from both their saliency maps and the image dataset (*e.g.*, knowledge

of the ground truth). Thus, model training is essential to supervised saliency models. However, training a model requires both enough training data and a long time for optimizing the parameters. Moreover, if a new candidate saliency model is added, the parameters of the integration model have to be retrained. Since saliency integration is already follow-up work after the computation of saliency models, it is naturally supposed to be fast and efficient instead of even more time-consuming.

Therefore, unsupervised models facilitate saliency integration to ease the computational burden of model training from supervised models. Unsupervised saliency integration models [19], [35] only rely on the knowledge of the candidate saliency models. But as unsupervised models lack ground truth information, computing the weight of each saliency model accurately becomes extremely difficult. In practice, the miss-measurement of the weights of saliency models to be combined causes lots of errors. Le Meur *et al.* [32] indicated in their studies that saliency aggregation models may decrease the performance, even when robust integration methods are used. This is true in many cases, for instance, when most of the saliency maps from candidate saliency models misjudge a region on an image, the result of saliency integration will be highly susceptible to error. Therefore, in this paper, our objective is to take advantage of the high efficiency of unsupervised methods, at the same time, to avoid miss-judgement by the majority of the candidate saliency models. Thus, we explore an unsupervised saliency integration approach with two principles:

1. **Rational expertise of models.** Saliency integration approach should give a rational measurement of the expertise of each saliency model to be combined, even though the ground truth is not provided.

2. **Solid performance enhancement.** Saliency integration approach should solidly outperform every one of the combined saliency maps, regardless of the choice of candidate saliency models.

Based on the above two principles, we propose a saliency integration framework based on the Bayes' probability theory, namely the arbitrator model (AM), which incorporates the prior and multiple saliency models with varying expertise. The arbitrator model introduces a reference saliency map based on generally accepted knowledge. Since either the multiple saliency models or the reference saliency map may misjudge a region on an image at the same time, the arbitrator makes a prudent judgement based on both the evidence and the reference, and exploits the prior map. Meanwhile, two methods are proposed to acquire the reliable expertise of each saliency model, one is probability based, the other is Expectation-Maximization (EM) based.

To acquire the prior map, we firstly compute a reference saliency map based on a widely accepted boundary-based measure in distinguishing the foreground from the background on an image. This reference map provides general knowledge about saliency information to the given multiple saliency maps (evidence) from saliency models. Then, we compute a prudent judgement map based on the consistency of the evidence and the reference, and expand the prior map from the judgement map. The expertise of different saliency models is then measured without ground truth. Lastly, we formulate a Bayes' probability based framework to incorporate the prior and evidence with varying expertise into a cellular automaton that leads the results to a stable state. The resulted stable saliency map is the final integrated saliency map. The framework of the proposed arbitrator model is illustrated in Figure 1.

The proposed AM model is evaluated on five challenging datasets under various combinations of state-of-the-art saliency models. The experimental results show that the AM model brings substantial improvement compared to the existing state-of-the-art approach. Moreover, all combinations of approaches consistently outperform the corresponding single ones, indicating that the proposed framework is independent of the choices of candidate saliency approaches.

The contributions of this paper are three-fold:

- (1) We incorporate a prior map and saliency models of varying expertise into a probability based framework to compute the final saliency map.
- (2) The proposed arbitrator model (AM) computes the prior map based on the consistency of the evidence from multiple saliency models and a reference saliency map from generally accepted knowledge.
- (3) We propose two methods to measure the expertise of multiple saliency models without any knowledge of the ground truth.

II. PROBABILITY-BASED SALIENCY ESTIMATION

Superpixel algorithms group pixels in an image with similar appearance features into perceptually consistent units, and thus can efficiently reduce the computational complexity of subsequent image processing tasks. Hence, in this work, we proceed all the information from saliency maps in superpixel units instead of pixel level.

Given an image of N superpixels, each superpixel has a unique saliency label $l_n \in \{0, 1\}$. We define the events that the n -th superpixel is salient (foreground) and inconspicuous (background) by F_n and \bar{F}_n respectively. Obviously, we have $P(F_n) = P(l_n = 1)$, while $P(\bar{F}_n) = 1 - P(F_n) = P(l_n = 0)$.

Suppose there are P evaluators (*i.e.*, saliency approaches), each of which is able to assign a saliency intensity $s_{p,n} \in [0, 1]$ to the n -th superpixel on the p -th saliency map. The binary saliency label of the n -th superpixel by the p -th evaluator, is denoted as $\iota_{p,n} \in \{0, 1\}$. $\iota_{p,n} = 1$ indicates the n -th superpixel is considered as a foreground one and vice versa. It can be easily obtained via a binarization process on the saliency intensity $s_{p,n}$ with a threshold γ_p , *e.g.*, OTSU thresholding [36]. More specifically, we have $\iota_{p,n} = 1$ ($\iota_{p,n}$),

if $s_{p,n} \geq \gamma_p$, otherwise, $\iota_{p,n} = 0$. Similarly, $\iota_{q \neq p,n} = 1$ ($\iota_{q \neq p,n}$), if $s_{q \neq p,n} \geq \gamma_p$, otherwise, $\iota_{q \neq p,n} = 0$. Given the saliency intensity of the n -th superpixel by the p -th evaluator $s_{p,n}$ and the n -th superpixels are labeled as foreground on the binary saliency maps by the rest of the evaluators $\iota_{q \neq p,n}$, the probability that the n -th superpixel by the p -th evaluator is measured as foreground is $P(F_n | s_{p,n}, \iota_{q \neq p,n})$. In this work, nevertheless the contexts with respect to F , \bar{F} , s and ι are upon a superpixel n , the sub-index n is omitted for clarity, unless otherwise stated.

The probability $P(F | s_p, \iota_{q \neq p})$ is derived under the Bayes's probability framework:

$$\begin{aligned} P(F | s_p, \iota_{q \neq p}) &\propto P(F) P(s_p, \iota_{q \neq p} | F) \\ &= P(F) P(s_p | F) P(\iota_{q \neq p} | s_p, F) \\ &= P(F) P(s_p | F) \prod_{q \neq p} P(\iota_q | F), \end{aligned} \quad (1)$$

with the assumption that all P evaluators make decisions independently, either with respect to the saliency intensity s or the binary saliency label ι .

The ratio of $\frac{P(F | s_p, \iota_{q \neq p})}{P(\bar{F} | s_p, \iota_{q \neq p})}$ is computed as follow:

$$\begin{aligned} \Lambda(F | s_p, \iota_{q \neq p}) &= \frac{P(F | s_p, \iota_{q \neq p})}{P(\bar{F} | s_p, \iota_{q \neq p})} \\ &= \frac{P(F) P(s_p | F)}{P(\bar{F}) P(s_p | \bar{F})} \prod_{q \neq p} \frac{P(\iota_q | F)}{P(\iota_q | \bar{F})} \end{aligned} \quad (2)$$

Then we compute the logarithm function of $\Lambda(F | s_p, \iota_{q \neq p})$ as:

$$\begin{aligned} \ln \Lambda(F | s_p, \iota_{q \neq p}) &= \ln \frac{P(F)}{P(\bar{F})} + \ln \frac{P(s_p | F)}{P(s_p | \bar{F})} + \sum_{q \neq p} \ln \frac{P(\iota_q | F)}{P(\iota_q | \bar{F})} \end{aligned} \quad (3)$$

The target $P(F | s_p, \iota_{q \neq p})$ can be transformed from a logistic function of the left side of Eq. 3, after which the resulted $P(F | s_p, \iota_{q \neq p})$ will always be in the range of $[-1, 1]$.

In Eq. 3, $P(F)$ is regarded as the prior, and hence a prior map will be introduced. $\frac{P(s_p | F)}{P(s_p | \bar{F})}$ is the expertise of the p -th saliency intensity map, namely α_p , while $\frac{P(\iota_p | F)}{P(\iota_p | \bar{F})}$ is the expertise of the p -th binary saliency map, namely β_p .

The proposed arbitrator model (AM) is originally induced from Eq. 3, which incorporates both the prior $P(F)$ and the expertise of saliency models α_p and β_p . In the remaining parts of this section, we will introduce the methods utilized to compute each item in Eq. 3 in details. Moreover, as a solution for the arbitrator model to refine the prior and saliency models of varying expertise to a stable state, the generation of cellular automaton based on Eq. 3 will be presented.

A. Estimation of a prior map

Typically, a saliency integration model holds knowledge from the multiple saliency models, which is termed as the evidence in our arbitrator model. However, when most of the evidence misjudge a region on an image, the saliency integration model will be misguided by the evidence. Hence,

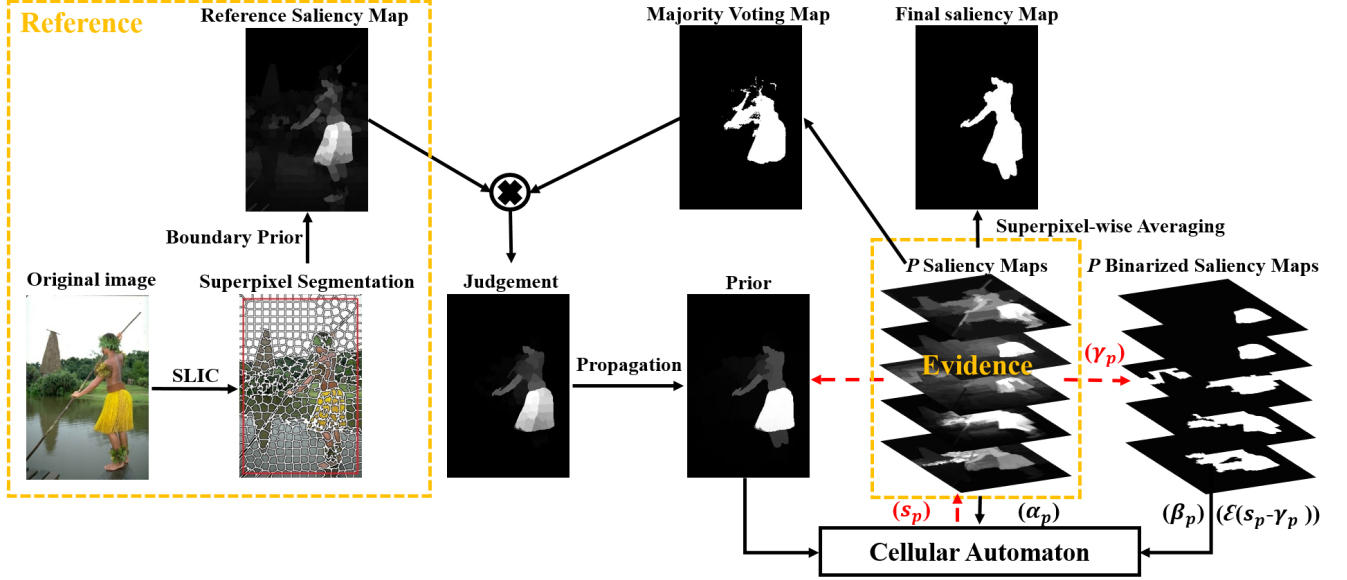


Fig. 1: Framework of the proposed AM model. The arbitrator incorporates the evidence from multiple saliency models and a reference map based on generally accepted knowledge, to make a prudent judgement, then computes a prior map. A probability based framework incorporates the prior map, P saliency maps of different expertise and P binarized saliency maps of different expertise into cellular automaton (CA), to compute the final result. α_p and β_p are the expertise of the p -th saliency intensity map and the p -th binarized map respectively. The saliency intensity values on the p -th saliency intensity map are updated by CA at each generation, accordingly the threshold γ_p is updated. $\mathcal{E}(s_p - \gamma_p)$ thresholds the p -th saliency intensity map to $\{-1, 1\}$ at each generation. The red dashed arrows point to the maps and parameters that are updated after each generation.

our arbitrator model introduces a reference saliency map from generally accepted knowledge and hears voices from both the evidence and the reference to make a prudent judgement.

In recent saliency detection approaches, it is widely accepted that the boundaries of a given image are most likely to be the background regions. Wei *et al.* [16], [37] pointed out that the most background regions, other than salient ones, are easily connected to image boundaries. Similarly, a number of saliency models [19], [38] generated a coarse saliency map with the compactness of image boundaries. Besides, several supervised saliency models [25], [39] also extracted the appearance features of boundaries for model training. Therefore, we compute a reference saliency map S_{Ref} based on this boundary prior knowledge. We assume that the more discrepant a superpixel is from the boundary superpixels, the more salient the superpixel is. We describe the mean CIE Lab feature of the n -th superpixel on an image as $\{c_n\}$ and select the superpixels along the four boundaries as boundary seeds. The boundary seeds are grouped into K clusters by K-means algorithm, c_b^k is the boundary superpixel belonging to the k -th cluster, K is empirically set as 3. For each superpixel c_n , we compute its appearance similarities to each cluster. If the superpixel is still quite different from its most similar cluster, it is more likely to be salient. In this way, we obtain the reference saliency map S_{Ref} :

$$S_{\text{Ref}}(c_n) = \min_{k \in \{1, \dots, K\}} \left(\frac{1}{N_k} \sum_{b=1}^{N_k} \|c_n - c_b^k\| \right), \quad (4)$$

where N_k is the number of superpixels in the k -th cluster,

$\|c_n - c_b^k\|$ computes the Euclidean distance between c_n and c_b^k .

In order to make a prudent decision, the arbitrator judges the superpixel as salient only if the majority of the evidence vote it as salient as well as the reference confirms its saliency. Given P saliency maps, $S_p(s_n)$ is defined as the mean intensity value of the n -th superpixel on the p -th saliency map. The majority voting evidence map is computed as

$$S_{\text{Maj}}(s_n) = \begin{cases} 1, & \sum_{p=1}^P \iota_{p,n} > \frac{P}{2} \\ 0, & \text{otherwise} \end{cases} \quad (5)$$

A prudent judgement S_{Judge} is computed by hearing voices from both the majority voting evidence map and the reference map:

$$S_{\text{Judge}} = S_{\text{Ref}} \times S_{\text{Maj}}, \quad (6)$$

The S_{Judge} is a saliency map of high precision that only holds saliency information for a certain parts of the image, so that we need to expand the saliency information to the whole image. A propagation method is employed to diffuse these saliency values on the prudent judgement map to the whole image iteratively. The over-segmented image can be regarded as an undirected graph $G = (V, E)$, which comprises a set V of the superpixels together with a set E of edges representing the similarity between adjacent superpixels. The constructed graph G can be described as an adjacent matrix $W = [w_{nm}]_{N \times N}$. In this work, the similarity between two superpixels is computed as $w_{nm} = \exp(-\mathcal{G}(c_n, c_m)^2 / (2\theta^2))$,

where θ is set as 0.25 and $\mathcal{G}(c_n, c_m)$ computes the geodesic distance between superpixel c_n and c_m as follows:

$$\mathcal{G}(c_n, c_m) = \min_{V_1=n, V_2, \dots, V_r=m} \left[\sum_{k=1}^{r-1} \max(\|V_k - V_{k+1}\| - a, 0) \right] \quad (7)$$

s.t. $V_k, V_{k+1} \in V$, V_k and V_{k+1} are connected in G , $\|V_k - V_{k+1}\|$ computes the Euclidean distance between V_k and V_{k+1} , and a is an adaptive threshold preventing the “small-weight-accumulation” problem [23], [37]. The $\mathcal{G}(c_n, c_m)$ measures the shortest path between c_n and c_m in the undirected graph G .

Finally, we use a propagation function as follow to compute the prior map:

$$S^{t+1} = I \cdot D^{-1} \cdot W \cdot S^t, \quad (8)$$

where I is the identity matrix and D is the diagonal degree matrix with $D_{nm} = \sum_m w_{nm}$, the initial $S^{t=0} = S_{\text{judge}}$, and after T_1 times of iterations, the final propagated S^{T_1} is computed as the prior map S_{Prior} .

B. Expertise of saliency models

The α_p and β_p measure the expertise of the p -th saliency model. α_p represents the expertise of the p -th saliency intensity map, which is a map with continuous values in the range of $[0, 1]$. β_p represents the expertise of the p -th binarized saliency map, which is a map with binary values $\{0, 1\}$.

In this paper, we propose two approaches to obtain the expertise of saliency models, one is a probability-based method from the intrinsic implications of Eq. 3, the other is an Expectation-Maximization (EM) method for evaluating multiple evaluators.

a. Probability-based expertise. According to the probabilistic framework of Eq. 3, we propose a natural way of evaluating the expertise α_p and β_p . β_p is originally derived from $\frac{P(\iota_p|F)}{P(\iota_p|\bar{F})}$. More specifically, $P(\iota_p|F)$ is actually $P(\iota_{p,n} = 1|F_n)$, indicating the probability that the n -th superpixel on the p -th saliency map is labeled as foreground given the superpixel is a foreground one. Similarly, $P(\iota_p|\bar{F})$ is originally $P(\iota_{p,n} = 1|\bar{F}_n)$, indicating the probability that the n -th superpixel is labeled as foreground given the superpixel is a background one. Thus, $P(\iota_{p,n} = 1|F_n)$ and $P(\iota_{p,n} = 1|\bar{F}_n)$ can be obtained only based on their intrinsic implications, and the corresponding $\beta_{p,n}$ with respect to the n -th superpixel is then computed. In this work, as the burden of computing every local $\beta_{p,n}$ is high, we set a threshold λ to classify the prior map $P(F)$ as foreground or background samples, and estimate a global β_p to approximate the expertise of all the superpixels on the p -th saliency map.

α_p , or $\frac{P(s_p|F)}{P(s_p|\bar{F})}$, can be computed in a similar way as computing β_p . However, as s_p is a map with continuous values other than discrete ones, we employ a fixed stepsize of 0.1 in $[0.1, 0.9]$ to binarize s_p with nine gradually increasing thresholds, and the corresponding α_p is the mean ratio of $\frac{P(\iota_p|F)}{P(\iota_p|\bar{F})}$ at all the stepsizes.

b. EM-based expertise. Motivated by Whitehill *et al.* [40], besides the assumption that evaluators vary in expertise (α_p and β_p), we presume that each superpixel in an image has varying degrees of difficulty for saliency assessment and introduce a measurement π_n to represent the difficulty of a superpixel. More skilled evaluators (higher α_p and β_p) have a higher probability of correctly labeling an image. As the difficulty π_n of a superpixel increases, the probability of correctly labeling the superpixel decreases, and vice versa. Thus, the probability that the p -th evaluator correctly labels a superpixel on an image is

$$p(\iota_{p,n} = l_n | \beta_p, \pi_n) = \frac{1}{1 + e^{-\beta_p/\pi_n}}, \quad (9)$$

where l_n are conditional independent hidden variables, while β_p and π_n are parameters. The Expectation-Maximization (EM) algorithm is used to achieve the optimal values of the hidden variables. More specifically, in the Expectation step, the expected value of the log likelihood function with respect to the conditional distribution of $\mathbf{l} = \{l_n\}$ given $\boldsymbol{\iota} = \{\iota_{p,n}\}$ under the current estimate of $\boldsymbol{\beta} = \{\beta_p\}$ and $\boldsymbol{\pi} = \{\pi_n\}$ is calculated as follows:

$$\begin{aligned} Q(\boldsymbol{\theta}) &= E[\ln p(\boldsymbol{\iota}, \mathbf{l} | \boldsymbol{\theta})] \\ &= E \left[\ln \prod_n \left(p(l_n) \prod_p p(\iota_{p,n} | l_n, \beta_p, \pi_n) \right) \right] \\ &= \sum_n E[\ln p(l_n)] + \sum_{p,n} E[\ln p(\iota_{p,n} | l_n, \beta_p, \pi_n)], \end{aligned} \quad (10)$$

where $\boldsymbol{\theta}$ refers to all parameters included in $\boldsymbol{\beta}$ and $\boldsymbol{\pi}$ for clarity.

In the Maximization step, the parameter settings of $\boldsymbol{\theta}$ are found to maximize the quantity function Eq. 10.

$$\tilde{\boldsymbol{\theta}} = \arg \max_{\boldsymbol{\theta}} Q(\boldsymbol{\theta}). \quad (11)$$

In this work, we presume that α_p is equal to β_p to simplify the computation, and the details of the EM algorithm can be found in [40].

C. Cellular automaton: a solution for integration

With the prior map and saliency models of varying expertise, the arbitrator model eventually incorporates all these elements to generate a final saliency map. In this work, we adopt cellular automaton for the final integration.

Cellular Automaton (CA), *a.k.a.*, cellular space or homogeneous structure, is a discrete model in computability theory and mathematics [19], [41]–[43]. A CA consists of a regular grid of cells. Each cell is with states, which are either discrete (*e.g.*, ‘On’ and ‘Off’) [41]–[43] or continuous (*e.g.*, between 0 and 1) [19]. A set of cells, namely neighborhood, is defined with respect to each cell. The neighborhood of one specific cell can influence the states of the specific cell in next generations (advancing t by 1) in line with certain updating rules. Generally, the rule of updating the state of cells is a mathematical function, which is usually synchronous to all cells and time invariants. Based on Stephen Wolfram’s theory [42], CA rules can be classified into four types. After evolving the updating rule, the state of evolved cells will reach

1) a stable state; 2) oscillating structures; 3) a chaotic pattern; or 4) complex localized structures.

In this work, we regard each superpixel as the cell and the superpixels at the same locations in different saliency maps are neighborhood, and then derive the synchronous updating rule of cellular automaton from Eq. 3 as follows:

$$\begin{aligned} \text{logit}(s_p^{t+1}) = & \text{logit}(S_{\text{Prior}}^t) \\ & + \ln(\alpha_p^t) \cdot s_p^t \\ & + \sum_{q \neq p} \ln(\beta_q^t) \cdot \mathcal{E}(s_q^t - \gamma_p^t), \end{aligned} \quad (12)$$

where α_p^t , β_q^t and γ_p^t are computed at each generation t based on s_p^t and s_q^t . $\mathcal{E}(x) = 1$, if $x > 0$, otherwise $\mathcal{E}(x) = -1$. $S_{\text{Prior}}^{t=0}$ is defined as the prior S_{Prior} computed in Section II-A, and at generation t ,

$$S_{\text{Prior}}^t = \frac{1}{P} \sum_{p=1}^P s_p^t. \quad (13)$$

The defined updating rule belongs to the type 1. After T_2 times of generations, all the saliency intensity maps $s_p^{T_2}, p = 1, \dots, P$ will converge into stable states, then we compute the final saliency map as follow:

$$S_{\text{Final}} = \frac{1}{P} \sum_{p=1}^P s_p^{T_2}. \quad (14)$$

III. EXPERIMENTS

The proposed arbitrator model (AM) aims at generating a saliency integration approach that solidly enhances the performance regardless of the choice of candidate saliency models. Thus, we perform a comprehensive analysis of the AM model by collecting a pool of twenty-two state-of-the-art saliency models as the candidate models for selection of combination, and evaluate the AM model with various combination strategies. The twenty-two collected saliency models include BSCA [19], CA [44], CEOS [45], COV [27], DRFI [39], FT [9], GBVS [5], GC [14], GP [46], HS [47], IS [29], IT [4], LR [30], MB [48], MB+ [48], MR [49], PCAS [28], RB [37], RC [14], SR [8], TLLT [23], and UFO [39]. The implementations of the chosen approaches are directly from the corresponding authors.

For comprehensive evaluation, five challenging datasets are utilized in the experiments: ECSSD [47], PASCAL-S [50], ASD [9], ImgSal [51] and DUT-OMRON [49]. The ASD dataset is one of the most widely used datasets with 1000 images from the MSRA-5000 Saliency Object Database [52], with distinct salient objects on the scenes. The PASCAL-S is a dataset of 850 images from PASCAL VOC 2010 [53] with multiple salient objects on the scenes. The ImgSal dataset is challenging, including 235 images in six levels of complexity. The ECSSD dataset contains 1000 images with complex salient objects on the scenes, and the objects on the images are semantically meaningful. The DUT-OMRON dataset contains a large number of 5168 more difficult and challenging images.

A. Implementation and evaluation

We over-segment the images into $N = 400$ superpixels with the simple linear iterative clustering (SLIC) algorithm [54]. In practice, T_1 is set as 5, T_2 is set as 5, and λ is set as 0.1. We reference our arbitrator model with probability-based expertise as AM-P and with EM-based expertise as AM-E in all the experiments. Besides the saliency maps computed from AM-P and AM-E, we also compute the average saliency maps of the combined saliency models (AVE), and saliency maps of the state-of-the-art unsupervised saliency integration model MCA [19] for fair comparisons.

We employ two types of evaluation metrics to evaluate the performance of saliency maps: F-measure and mean absolute error (MAE). When a given saliency map is slidingly thresholded from 0 to 255, a precision-recall (PR) curve can be computed based on the ground truth. F-measure is computed to count for the saliency maps with both high precision and recall:

$$F = \frac{(1 + \beta^2) \cdot \text{precision} \cdot \text{recall}}{\beta^2 \cdot \text{precision} + \text{recall}}, \quad (15)$$

where $\beta^2 = 0.3$ [9] to emphasize the precision.

MAE measures the overall pixel-wise difference between the saliency map sal and the ground truth gt : $\text{MAE} = \frac{1}{H} \sum_{h=1}^H |sal(h) - gt(h)|$, H is the number of pixels on the map.

Table I lists the performance of the collected saliency models from the model pool. To save the space, we code each model with a capital letter. The models are illustrated by ranking their F-measure and their MAE scores are also presented correspondingly.

B. Comparisons of various combinations

We investigate our AM saliency integration model by evaluating more than fifty combinations, and various numbers of candidate saliency models are integrated in the experiments. The experimental results are evaluated on ECSSD dataset, and we choose the number of candidate saliency models for integration from 2 to 8. If enumerating all the possible combinations from 2 to 8 models, we need to evaluate $C_{22}^2 + C_{22}^3 \dots + C_{22}^8 = 600,347$ combinations, which is almost impossible. Thus, we follow three different strategies to evaluate the representative combinations.

1. **Superior models combination.** We rank the F-measure of the twenty-two saliency models as shown in Table I. When choosing the candidate saliency models, we only consider those saliency models with the best performance. Thus, we choose two best-performed saliency models for 2-model-combination, three best-performed saliency models for 3-model-combination and so forth. The first seven rows in Table II indicate the evaluation results, where it can be easily perceived that both AM-P and AM-E outperform the top candidate saliency model as well as the MCA model in every combination. Thus, the proposed AM model performs well when superior saliency models are combined, and AM-E slightly outperforms AM-P.

Model	MB+	GP	MB	BSCA	DRFI	TLLT	RC	MR	HS	RB	UFO
Code Letter	A	B	C	D	E	F	G	H	I	J	K
F-measure	.652	.619	.617	.605	.592	.590	.580	.578	.571	.568	.487
MAE	.171	.191	.174	.183	.171	.172	.186	.187	.228	.172	.203

Model	GC	PCAS	LR	GBVS	COV	IT	CA	IS	CEOS	SR	FT
Code Letter	L	M	N	O	P	Q	R	S	T	U	V
F-measure	.485	.426	.422	.406	.358	.358	.346	.308	.277	.276	.246
MAE	.235	.247	.274	.263	.220	.289	.309	.334	.716	.311	.291

TABLE I: The collected saliency models from the model pool. Each model is coded with a capital letter. The models are ranked by their F-measure and their MAE scores are also illustrated.

No.	Combination	F-measure					MAE				
		Top	AVE	MCA	AM-P	AM-E	Top	AVE	MCA	AM-P	AM-E
1	A B	.652	.595	.665	<u>.710</u>	.717	.171	.181	.162	.134	.134
	A B C	.652	.624	.675	<u>.705</u>	.713	.171	.179	.154	<u>.138</u>	.136
	A B C D	.652	.616	.694	<u>.717</u>	.720	.171	.180	.144	.132	<u>.133</u>
	A B C D E	.652	.605	.720	<u>.735</u>	.739	.171	.177	.132	<u>.125</u>	.124
	A B C D E F	.652	.595	.726	.743	<u>.742</u>	.171	.176	.128	.122	<u>.124</u>
	A B C D E F G	.652	.589	.735	<u>.747</u>	.749	.171	.177	.124	.120	.120
	A B C D E F G H	.652	.585	.736	<u>.743</u>	.745	.171	.178	.123	<u>.122</u>	.121
2	U V	.291	.222	.288	.438	<u>.415</u>	.291	.306	.279	<u>.228</u>	.214
	T U V	.277	.277	.435	<u>.545</u>	.579	.291	.287	.231	<u>.195</u>	.178
	S T U V	.308	.275	.461	<u>.541</u>	.554	.291	.299	.231	<u>.196</u>	.188
	R S T U V	.346	.281	.487	<u>.547</u>	.574	.291	.301	.229	<u>.197</u>	.187
	Q R S T U V	.358	.287	.518	<u>.561</u>	.586	.289	.302	.219	<u>.191</u>	.182
	P Q R S T U V	.358	.282	.546	<u>.576</u>	.610	.220	.293	.202	<u>.187</u>	.175
	O P Q R S T U V	.406	.295	.570	<u>.589</u>	.623	.228	.289	.194	<u>.181</u>	.170
3	B E	.619	.595	.668	.760	<u>.754</u>	.171	.181	.152	.114	<u>.119</u>
	I Q S	.571	.375	.545	<u>.659</u>	.670	.228	.286	.215	<u>.161</u>	.153
	I L R U	.578	.371	.556	.624	<u>.613</u>	.187	.271	.199	.167	<u>.169</u>
	H I L P R	.617	.420	.639	<u>.683</u>	.698	.174	.235	.160	<u>.143</u>	.138
	B D O P V G	.652	.434	.678	<u>.698</u>	.710	.174	.217	.148	<u>.143</u>	.140
	A B D J O Q S	.652	.474	.693	<u>.717</u>	.721	.171	.227	.142	<u>.133</u>	.131
	C D F L M O I R	.652	.470	.702	<u>.714</u>	.716	.172	.225	.138	.133	<u>.134</u>

TABLE II: F-measure and MAE scores of the average saliency maps (AVE), the resulted MCA saliency maps and the resulted AM-P and AM-E saliency maps. The first column shows the combination strategy, and for every combination the highest F-measure and lowest MAE score of the candidate saliency models are displayed in the “Top” column. The best result for each combination is in bold, while the second best is underlined.

2. **Inferior models combination.** We only consider those saliency models with the worst performance. Thus, we choose the worst two saliency models for 2-model-combination, the worst three saliency models for 3-model-combination and so forth. The results in group No.2 of Table II present the evaluation results. When the candidate saliency models for integration show inferior performances, our AM model largely improves the F-measure of the top candidate saliency model with an average increase of 22.6% for AM-P and 28.9% for AM-E. Apparently, our AM model greatly rectifies the error saliency information from the inferior candidate saliency models, and AM-E performs even better than AM-P for inferior models combinations.

3. **Random combination.** From 2-model combination to 8-model combination, we randomly select candidate saliency models from the model pool and randomly evaluate five different combinations for each fixed number combination. The last seven rows in Table II show one example of each fixed number combination with random selection strategy.

Again, our proposed AM model consistently outperforms each one of the combined saliency models and the MCA model. Figure 2 indicates the performance enhancement of average maps, MCA model, AM-P and AM-E model compared to the corresponding top models by averaging five random combinations of candidate saliency models. Apparently, the proposed model solidly improves the performance independent of the number of models being chosen for combination.

C. Experiments on five datasets

We evaluate our AM model over five challenging datasets, ECSSD, PASCAL-S, ASD, ImgSal, and DUT-OMRON. We choose a combination used on ECSSD dataset from Section III-B and evaluate this combination on the other four datasets. The chosen models being integrated are GP, MB+, UFO, PCAS, LR and GBVS. Table III presents the F-measure and MAE of the top performed candidate saliency models, average saliency maps, MCA results and our AM results over the five datasets. The MCA model can not outperform the

Dataset	F-measure					MAE				
	Top	AVE	MCA	AM-P	AM-E	Top	AVE	MCA	AM-P	AM-E
ECSSD	.651	.482	.686	.714	.713	.171	.223	.147	.136	.136
ASD	.711	.478	.705	<u>.818</u>	.858	.110	.186	.110	<u>.071</u>	.064
ImgSal	.438	.282	.428	.516	<u>.513</u>	.117	.195	.126	<u>.092</u>	.089
DUT-OMRON	.526	.393	.534	.576	<u>.573</u>	.170	.214	.147	<u>.126</u>	.124
PASCAL	.420	.370	.572	.591	.591	.226	.258	.207	.198	.198

TABLE III: F-measure and MAE scores of the top performed saliency model, average saliency maps, MCA model, and AM model with a combination of GBVS, GP, LR, MB+, PCAS and UFO models on five datasets including ECSSD, ASD, ImgSal, DUT-OMRON and PASCAL-S.

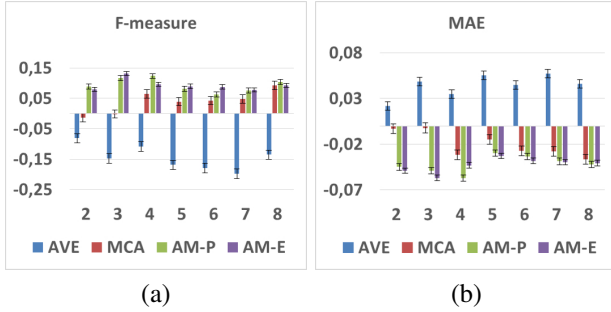


Fig. 2: The average performance enhancement of five randomly selected combinations of strategy 3 in Section III-B compared to their corresponding top models. (a) measures the average F-measure improvement. (b) measures the average reduction of MAE score. The average maps, MCA results, AM-P and AM-E results are compared and the numbers in horizontal axis indicate the number of candidate models being combined.

best candidate saliency models on ASD and ImgSal datasets, while our AM model largely improves the performance of the best candidate model on all the five datasets. Generally, the AM-P model results in higher F-measure, but AM-E gives better MAE scores. Figure 3 (a)-(e) present the average precision, recall, and F-measure of the saliency maps being combined, the average saliency maps, results from MCA model and results from the proposed AM model on the five datasets. Generally, the proposed AM model possesses both high precision and recall, but emphasizes more on precision. Figure 4 shows some examples of the results of candidate saliency models, the average saliency maps, MCA model and the proposed AM model on the five datasets.

D. Discussion of convergence

As mentioned in Section II-C, the synchronizing updating rule of the cellular automaton is designed to converge the evolved cells to a stable state after several generations. We compute the absolute difference of the S_{Prior}^t and S_{Prior}^{t-1} in Eq. 13 at each generation, and plot the average absolute difference between S_{Prior}^t and S_{Prior}^{t-1} of all the superpixels on one image, with the same combination used in Section III-C on ECSSD dataset. The result is illustrated on Figure 3 (f). As is shown, the designed updating rule for cellular automaton can make the S_{Prior}^t rapidly converge within five iterations.

E. Running time

The experimental environment is under Windows system with an i5-3570 CPU at 3.40GHz, and MATLAB R2014b is the implementation tool. In practice, the running time of AM-P on ECSSD dataset ranges from 1.28s (2-model-combination) to 1.32s (8-model-combination) per image, while AM-E ranges from 1.38s (2-model-combination) to 2.06s (8-model-combination), without code optimization. The AM-E and AM-P show comparable performances, but AM-E takes longer time in running the EM algorithm.

IV. CONCLUSION

In this paper, we propose an unsupervised saliency integration model, namely the arbitrator model (AM), which releases the burden of model-training from supervised models. On one hand, the AM overcomes the misleading of inferior saliency models by exploring the consistency of the evidence from multiple saliency maps and a reference saliency map from generally accepted knowledge, on the other, it rationally learns the expertise of saliency models without any knowledge of the ground truth. The experimental results show that the AM model substantially improves the performance, regardless of the choices of candidate approaches, indicating that the proposed AM model is state-of-the-art.

REFERENCES

- [1] E. Rahtu, J. Kannala, M. Salo, and J. Heikkilä, "Segmenting salient objects from images and videos," in *Proc. ECCV*, 2010, pp. 366–379.
- [2] C. Guo and L. Zhang, "A novel multiresolution spatiotemporal saliency detection model and its applications in image and video compression," *TIP*, vol. 19, no. 1, pp. 185–198, 2010.
- [3] X.-S. Hua, T. Mei, and S. Li, "When multimedia advertising meets the new internet era," in *Workshop on Multimedia Signal Processing*. IEEE, 2008, pp. 1–5.
- [4] L. Itti, C. Koch, and E. Niebur, "A model of saliency-based visual attention for rapid scene analysis," *TPAMI*, vol. 20, no. 11, pp. 1254–1259, 1998.
- [5] J. Harel, C. Koch, and P. Perona, "Graph-based visual saliency," in *NIPS*, 2006, pp. 545–552.
- [6] D. Walther and C. Koch, "Modeling attention to salient proto-objects," *Neural Networks*, vol. 19, no. 9, pp. 1395–1407, 2006.
- [7] N. Bruce and J. Tsotsos, "Saliency based on information maximization," in *NIPS*, 2005, pp. 155–162.
- [8] X. Hou and L. Zhang, "Saliency detection: A spectral residual approach," in *Proc. CVPR*. IEEE, 2007, pp. 1–8.
- [9] R. Achanta, S. Hemami, F. Estrada, and S. Susstrunk, "Frequency-tuned salient region detection," in *Proc. CVPR*. IEEE, 2009, pp. 1597–1604.
- [10] T. Judd, K. Ehinger, F. Durand, and A. Torralba, "Learning to predict where humans look," in *Proc. ICCV*. IEEE, 2009, pp. 2106–2113.
- [11] M. Jiang, J. Xu, and Q. Zhao, "Saliency in crowd," in *Proc. ECCV*. Springer, 2014, pp. 17–32.

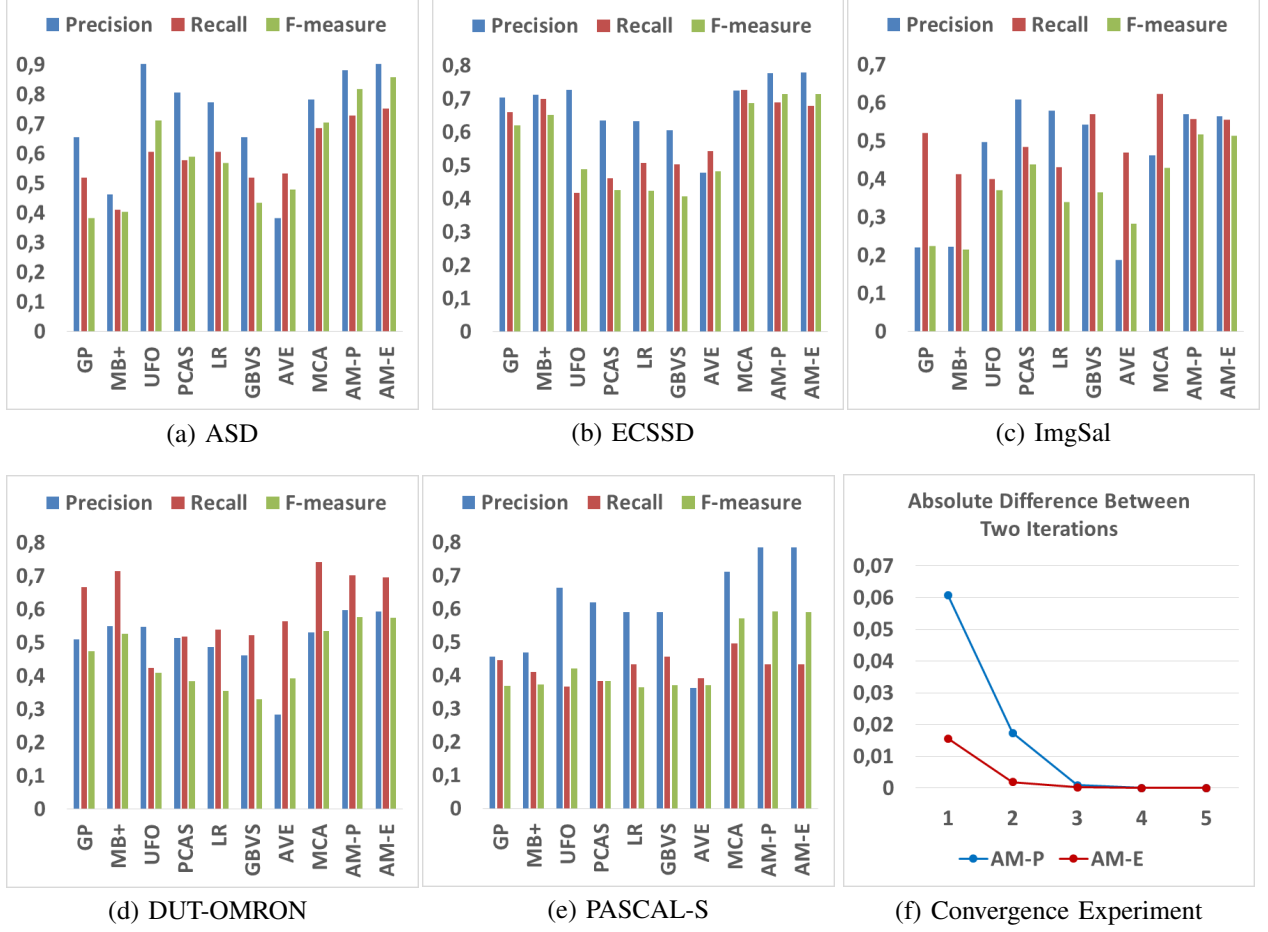


Fig. 3: (a)-(e) The average precision, recall, and F-measure of candidate saliency models, the average saliency maps, MCA model and the proposed AM model on the five datasets including ECSSD, PASCAL-S, ASD, ImgSal, and DUT-OMRON. (f) Convergence experiments computing the average absolute difference of all superpixels between two generations.

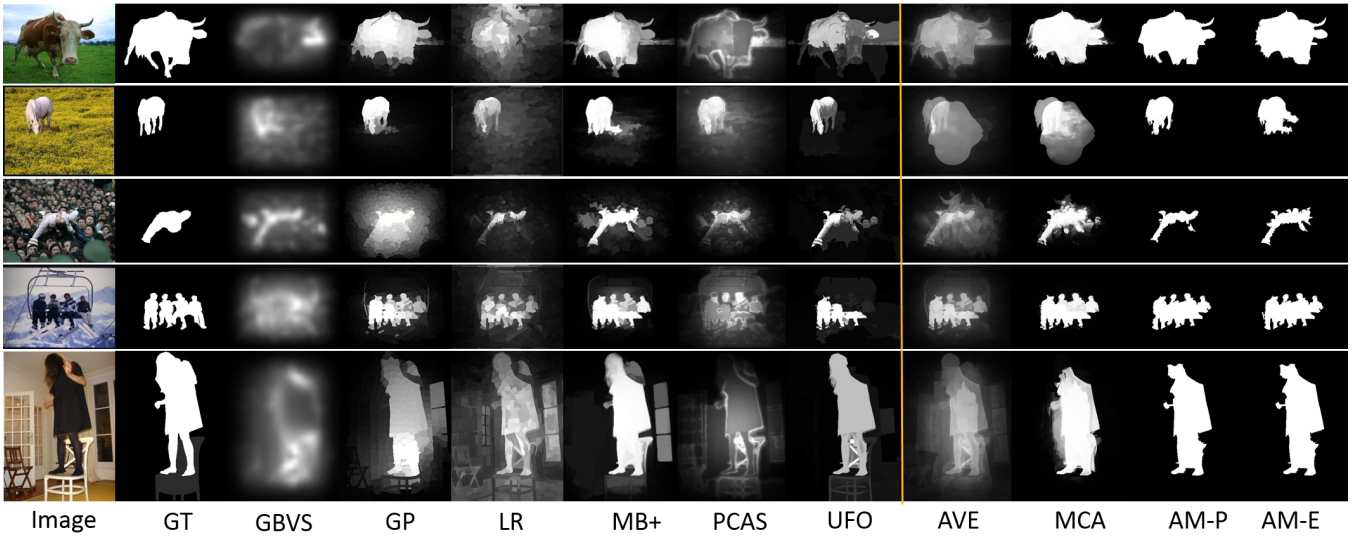


Fig. 4: Examples of the results of combined saliency models, average saliency maps (AVE), MCA, AM-P and AM-E. The images with ground truth (GT) are sequentially from ECSSD, ASD, ImgSal, DUT-OMRON and PASCAL-S datasets.

- [12] O. L. Meur, P. L. Callet, D. Barba, and D. Thoreau, "A coherent computational approach to model bottom-up visual attention," *TPAMI*, vol. 28, no. 5, pp. 802–817, 2006.
- [13] L. Zhang, M. H. Tong, T. K. Marks, H. Shan, and G. W. Cottrell, "Sun: A bayesian framework for saliency using natural statistics," *Journal of Vision*, vol. 8, no. 7, p. 32, 2008.
- [14] M. Cheng, N. J. Mitra, X. Huang, P. H. Torr, and S. Hu, "Global contrast based salient region detection," *TPAMI*, vol. 37, no. 3, pp. 569–582, 2015.
- [15] S. Lu, V. Mahadevan, and N. Vasconcelos, "Learning optimal seeds for diffusion-based salient object detection," in *Proc. CVPR*. IEEE, 2014, pp. 2790–2797.
- [16] W. Zhu, S. Liang, Y. Wei, and J. Sun, "Saliency optimization from robust background detection," in *Proc. CVPR*. IEEE, 2014, pp. 2814–2821.
- [17] T. Shi, M. Liang, and X. Hu, "A reverse hierarchy model for predicting eye fixations," in *Proc. CVPR*. IEEE, 2014, pp. 2822–2829.
- [18] R. Liu, J. Cao, Z. Lin, and S. Shan, "Adaptive partial differential equation learning for visual saliency detection," in *Proc. CVPR*, 2014, pp. 3866–3873.
- [19] Y. Qin, H. Lu, Y. Xu, and H. Wang, "Saliency detection via cellular automata," in *Proc. CVPR*. IEEE, 2015, pp. 110–119.
- [20] N. Liu, J. Han, D. Zhang, S. Wen, and T. Liu, "Predicting eye fixations using convolutional neural networks," in *Proc. CVPR*. IEEE, 2015, pp. 362–370.
- [21] R. Zhao, W. Ouyang, H. Li, and X. Wang, "Saliency detection by multi-context deep learning," in *Proc. CVPR*. IEEE, 2015, pp. 1265–1274.
- [22] N. Tong, H. Lu, X. Ruan, and M.-H. Yang, "Salient object detection via bootstrap learning," in *Proc. CVPR*. IEEE, 2015, pp. 1884–1892.
- [23] C. Gong, D. Tao, W. Liu, S. J. Maybank, M. Fang, K. Fu, and J. Yang, "Saliency propagation from simple to difficult," in *Proc. CVPR*. IEEE, 2015, pp. 2531–2539.
- [24] D. Zhang, J. Han, C. Li, and J. Wang, "Co-saliency detection via looking deep and wide," in *Proc. CVPR*, 2015, pp. 2994–3002.
- [25] L. Wang, H. Lu, X. Ruan, and M.-H. Yang, "Deep networks for saliency detection via local estimation and global search," in *Proc. CVPR*, 2015, pp. 3183–3192.
- [26] C. Kanan, M. H. Tong, L. Zhang, and G. W. Cottrell, "Sun: Top-down saliency using natural statistics," *Visual Cognition*, vol. 17, no. 6-7, pp. 979–1003, 2009.
- [27] E. Erdem and A. Erdem, "Visual saliency estimation by nonlinearly integrating features using region covariances," *Journal of Vision*, vol. 13, no. 4, p. 11, 2013.
- [28] R. Margolin, A. Tal, and L. Zelnik-Manor, "What makes a patch distinct?" in *Proc. CVPR*. IEEE, 2013, pp. 1139–1146.
- [29] X. Hou, J. Harel, and C. Koch, "Image signature: Highlighting sparse salient regions," *TPAMI*, vol. 34, no. 1, pp. 194–201, 2012.
- [30] X. Shen and Y. Wu, "A unified approach to salient object detection via low rank matrix recovery," in *Proc. CVPR*. IEEE, 2012, pp. 853–860.
- [31] C. Shen and Q. Zhao, "Webpage saliency," in *Proc. ECCV*, 2014, pp. 33–46.
- [32] O. Le Meur and Z. Liu, "Saliency aggregation: Does unity make strength?" in *Proc. ACCV*. Springer, 2014, pp. 18–32.
- [33] L. Mai, Y. Niu, and F. Liu, "Saliency aggregation: a data-driven approach," in *Proc. CVPR*, 2013, pp. 1131–1138.
- [34] J. Wang, A. Borji, C.-C. J. Kuo, and L. Itti, "Learning a combined model of visual saliency for fixation prediction," *TIP*, vol. 25, no. 4, pp. 1566–1579, 2016.
- [35] A. Borji, D. N. Sihite, and L. Itti, "Salient object detection: A benchmark," in *Proc. ECCV*. Springer, 2012, pp. 414–429.
- [36] N. Otsu, "A threshold selection method from gray-level histograms," *Automatica*, vol. 11, no. 285-296, pp. 23–27, 1975.
- [37] Y. Wei, F. Wen, W. Zhu, and J. Sun, "Geodesic saliency using background priors," in *Proc. ECCV*. Springer, 2012, pp. 29–42.
- [38] X. Li, H. Lu, L. Zhang, X. Ruan, and M.-H. Yang, "Saliency detection via dense and sparse reconstruction," in *Proc. ICCV*. IEEE, 2013, pp. 2976–2983.
- [39] H. Jiang, J. Wang, Z. Yuan, Y. Wu, N. Zheng, and S. Li, "Salient object detection: A discriminative regional feature integration approach," in *Proc. CVPR*, 2013, pp. 2083–2090.
- [40] J. Whitehill, T.-f. Wu, J. Bergsma, J. R. Movellan, and P. L. Ruvolo, "Whose vote should count more: Optimal integration of labels from labelers of unknown expertise," in *NIPS*, 2009, pp. 2035–2043.
- [41] J. Von Neumann, "The general and logical theory of automata," *Cerebral mechanisms in behavior*, pp. 1–41, 1951.
- [42] S. Wolfram, "Statistical mechanics of cellular automata," *Reviews of modern physics*, vol. 55, no. 3, p. 601, 1983.
- [43] —, "A new kind of science," *A new kind of science*, by Stephen Wolfram. Champaign, IL: Wolfram Media, 2002, ISBN 1579550088, vol. 1, 2002.
- [44] S. Goferman, L. Zelnik-Manor, and A. Tal, "Context-aware saliency detection," *TPAMI*, vol. 34, no. 10, pp. 1915–1926, 2012.
- [45] R. Mairon and O. Ben-Shahar, *A closer look at context: From coxels to the contextual emergence of object saliency*. Springer, 2014.
- [46] P. Jiang, N. Vasconcelos, and J. Peng, "Generic promotion of diffusion-based salient object detection," in *Proc. ICCV*, 2015, pp. 217–225.
- [47] Q. Yan, L. Xu, J. Shi, and J. Jia, "Hierarchical saliency detection," in *Proc. CVPR*, 2013, pp. 1155–1162.
- [48] J. Zhang, S. Sclaroff, Z. Lin, X. Shen, B. Price, and R. Mech, "Minimum barrier salient object detection at 80 fps," in *Proc. ICCV*, 2015, pp. 1404–1412.
- [49] C. Yang, L. Zhang, H. Lu, X. Ruan, and M.-H. Yang, "Saliency detection via graph-based manifold ranking," in *Proc. ICPR*, 2013, pp. 3166–3173.
- [50] Y. Li, X. Hou, C. Koch, J. M. Rehg, and A. L. Yuille, "The secrets of salient object segmentation," in *Proc. CVPR*. IEEE, 2014, pp. 280–287.
- [51] J. Li, M. D. Levine, X. An, X. Xu, and H. He, "Visual saliency based on scale-space analysis in the frequency domain," *TPAMI*, vol. 35, no. 4, pp. 996–1010, 2013.
- [52] T. Liu, Z. Yuan, J. Sun, J. Wang, N. Zheng, X. Tang, and H.-Y. Shum, "Learning to detect a salient object," *TPAMI*, vol. 33, no. 2, pp. 353–367, 2011.
- [53] M. Everingham, L. Van Gool, C. K. I. Williams, J. Winn, and A. Zisserman, "The PASCAL Visual Object Classes Challenge 2010 (VOC2010) Results," <http://www.pascal-network.org/challenges/VOC/voc2010/workshop/index.html>.
- [54] R. Achanta, A. Shaji, K. Smith, A. Lucchi, P. Fua, and S. Susstrunk, "Slic superpixels compared to state-of-the-art superpixel methods," *TPAMI*, vol. 34, no. 11, pp. 2274–2282, 2012.